Exploring the Threshold between Fullerenes and Nanotubes: Characterizing Isomerically Pure, Empty-Caged, and Tubular Fullertubes D_{5h} - C_{90} and D_{5d} - C_{100}

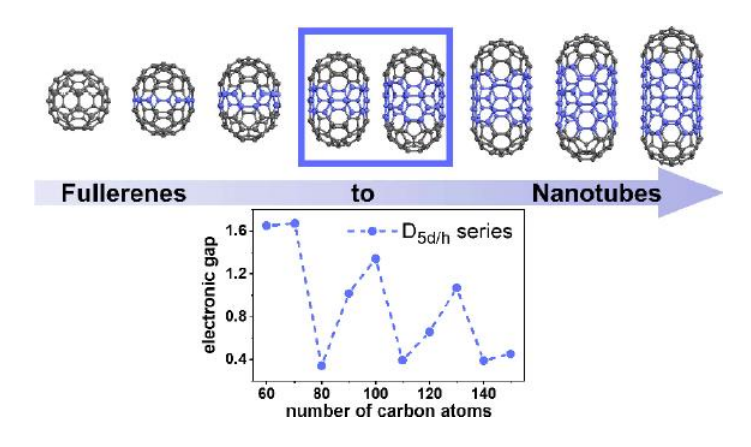
Christoph M. Schüßlbauer, ¹ Marcel Krug, ¹ Tobias Ullrich, ¹ Hannah M. Franklin, ² Steven Stevenson, ² Timothy Clark, ² and Dirk M. Guldi^{2,*}

- 1. Department of Chemistry and Pharmacy & Interdisciplinary Center of Molecular Materials (ICMM), Friedrich-Alexander-Universität Erlangen-Nürnberg, Erlangen 91058, Germany;
- 2. Department of Chemistry, Purdue University Fort Wayne, Fort Wayne, Indiana 46835, United States

*Corresponding Author

Abstract: We report the fully-fledged photophysical characterization of isomerically pure, empty-caged, tubular fullerenes D_{5h} - C_{90} and D_{5d} - C_{100} and compare their key properties. In particular, the focus was on cage sizes between 60 and 150 carbon atoms with D_3 , $D_{3d/h}$, and $D_{5d/h}$ symmetry. The optical band gap of D_{5d} - C_{100} is 1.65 eV, which is larger than 1.37 eV of D_{5h} - C_{90} . In stark contrast to the nonluminescent D_{5h} - C_{90} , D_{5d} - C_{100} luminesces at room temperature. Transient absorption spectroscopy shows that photoexcited D_{5d} - C_{100} is subject to a slow intersystem crossing that generates a triplet excited state. In contrast, a fast, nonradiative internal conversion governs the deactivation of D_{5h} - C_{90} : In this case, exploring the corresponding triplet excited state required triplet—triplet sensitization experiments with anthracene. Density functional theory calculations revealed the electronic structure of the fullertubes, and calculations are consistent with our experimental findings. The calculated band gap systematically decreases with the number of carbon atoms within the D_3 and $D_{3d/h}$ series. In contrast, an oscillating behavior is noted within the series of $D_{5d/h}$ fullertubes. Finally, photoexcited D_{5d} - C_{100} was found to undergo hole transfer with electron-donating triethylamines readily but not electron transfer with electron-accepting methyl viologens.

TOC Graphic:



Introduction:

Thirty years ago Krätschmer and Huffmann achieved a breakthrough in synthetic carbon allotrope research by reporting the large-scale synthesis of buckminsterfullerenes. ¹⁻³ Ever since, the most abundant fullerenes, C₆₀ and C₇₀, have been the two most intensely investigated nanocarbons. Applications range from materials science and medicinal chemistry to nanoscience and many more. ⁴ In the past, many investigations have focused on higher fullerenes up to C₈₄ and isomers thereof. Research on even higher fullerenes faces, however, two major impediments. The first is the drastically increasing number of isomers as the number of carbon atoms increases, and the second the limited solubility of higher empty-caged fullerenes. ^{5,6}

To overcome these hurdles, two strategies, exohedral and endohedral functionalization, have been used that allow isolation and characterization of higher fullerenes beyond C_{84} . Exohedral functionalization yields, for example, chlorinated fullerenes such as tubular C_{100} - Cl_{12} , C_{104} - Cl_{22} , and C_{108} - Cl_{12} . A major drawback of this approach is, however, that the electronic structure of the resulting fullerenes is heavily perturbed and bears little or no resemblance to that of pristine fullerenes. Endohedral functionalization based on encapsulating metals or metal carbides contributes to the stabilization of higher fullerenes. It relies on the transfer of electrons/charges from the encapsulated species to the fullerene. However, this endohedral functionalization also alters the electronic structure of the carbon framework through the redox reactions between cage and guest, even though the fullerene framework remains intact.

Recently, Stevenson *et al.* reported the isolation of the largest fullerenes to date; up to C_{156} , ¹² most notably the highly symmetrical D_{5h} - C_{90} and D_{5d} - C_{100} . Their tubular shape is essentially a structural combination of single-walled carbon nanotubes (SWCNTs) and fullerenes. Correspondingly, they are termed fullertubes. In an independent study, they also reported the further characterization of D_{5h} - C_{90} and D_{5d} - C_{100} by means of ¹³C NMR, XPS, and Raman spectroscopies. Raman and ¹³C NMR results were consistent with semi-conducting and metallic properties for D_{5h} - C_{90} and D_{5d} - C_{100} , respectively. ¹³

To date, the excited-state dynamics of empty-caged, tubular fullerenes beyond C_{84} remain completely unexplored. This is where the current work sets in. We report on the characterization of these recently isolated, isomerically pure nanotubular D_{5h} - C_{90} and D_{5d} - C_{100} . Additionally, to compare our experimental findings we investigated several series of tubular fullerenes up to C_{150} , by means of quantum chemical calculations. In a nutshell, tubular fullerenes with D_3 or $D_{3d/h}$ symmetries follow a trend of decreasing optical band gap with increasing cage size. In contrast, increasing the cage size of tubular fullerenes with $D_{5d/h}$ symmetry results in an oscillating optical band gap. Furthermore, our experimental results show that D_{5d} - C_{100} luminesces upon photoexcitation and is subject to slow intersystem crossing that results in the population of a triplet excited state. Photoexcited D_{5h} - C_{90} , on the other hand, deactivates via nonradiative internal conversion on a ps-time scale.

Results and Discussion:

 D_{5h} - C_{90} and D_{5d} - C_{100} were produced and isolated as reported recently by Stevenson et al.^{12,13} The ground-state electronic absorption spectra of D_{5h} - C_{90} in toluene and D_{5d} - C_{100} in carbon disulfide (CS₂) are shown in Figure 1a. Dilute solutions of D_{5h} - C_{90} are yellow and feature strong absorptions all the way up to 600 nm with major maxima at 327, 338, 376, 418, 478, and 583 nm. The latter tails off on in the red with an absorption onset at around 920 nm.

Overall, the absorption spectra are in sound agreement with those reported previously. 12,14 The ground-state absorption spectrum of D_{5d} - C_{100} in CS_2 features major absorptions at 411, 573, and 661 nm, followed by a low-intensity 755 nm shoulder and an absorption onset at 780 nm. The strong maximum in the visible range lends D_{5d} - C_{100} a purple color in solution. This renders it potentially useful as photosensitizer and/or building block in charge-transfer systems. Absorption spectra recorded in o-xylene are virtually identical to those found in CS_2 for D_{5d} - C_{100} except that all maxima are blue-shifted by approximately 4 nm (see Figure S8).

 D_{5h} - C_{90} lacks any detectable fluorescence. In contrast, D_{5d} - C_{100} reveals fluorescence beyond 750 nm with 765 and 900 nm maxima. Saturating CS_2 solutions of D_{5d} - C_{100} with dioxygen rather than nitrogen strongly quenches the D_{5d} - C_{100} fluorescence (Figure S9). At the same time, we detected fluorescence at 1270 nm, which we assign to the photoluminescence characteristics of singlet dioxygen. In fact, an excitation spectrum taken at 1270 nm is a perfect match to the D_{5d} - C_{100} absorption spectrum (Figure S10). Singlet dioxygen sensitization implies, however, the presence of a photo-sensitizer in its triplet excited state. Accordingly, we postulate that D_{5d} - C_{100} deactivates, at least in part, via intersystem crossing. This is in stark contrast to the trend observed for higher fullerenes smaller than D_{5d} - C_{100} , which give negligible triplet quantum yields. No singlet dioxygen photoluminescence was detected upon photoexcitation of dioxygen-saturated solutions of D_{5h} - C_{90} in, for example, toluene.

Next, we turned to the excitation energy gaps. The lack of fluorescence for D_{5h} - C_{90} made it necessary to derive its excitation energy gap from the 920 nm absorption onset to give a value of 1.34 eV in toluene. For D_{5d} - C_{100} , we used the long-wavelength absorption and the shortwavelength fluorescence to derive a value of 1.61 eV.

Our experimental results encouraged us to revisit the theoretical predictions for higher fullerenes. First, we looked into the electronic structure of I_h - C_{60} and D_{5h} - C_{70} to benchmark our density functional theory (DFT) calculations (see Supporting Information (SI) section 3.2 for details). Pure density functionals, such as BLYP, 17 provide reasonable quantitative values for the HOMO–LUMO and electrochemical gaps (see SI sections 3.2 and 3.4 for details). Optical gaps are best predicted through time-dependent DFT calculations with hybrid functionals with small proportions of Hartree–Fock exchange, for example, B3LYP, 18 TPSSh, 19 or PBE1PBE. 20 In excellent agreement with the experimental results, the TD-B3LYP/def2-SVP band gaps, that is, the lowest vertical transition, are for D_{5h} - C_{90} and D_{5d} - C_{100} 1.37 and 1.65 eV, respectively.

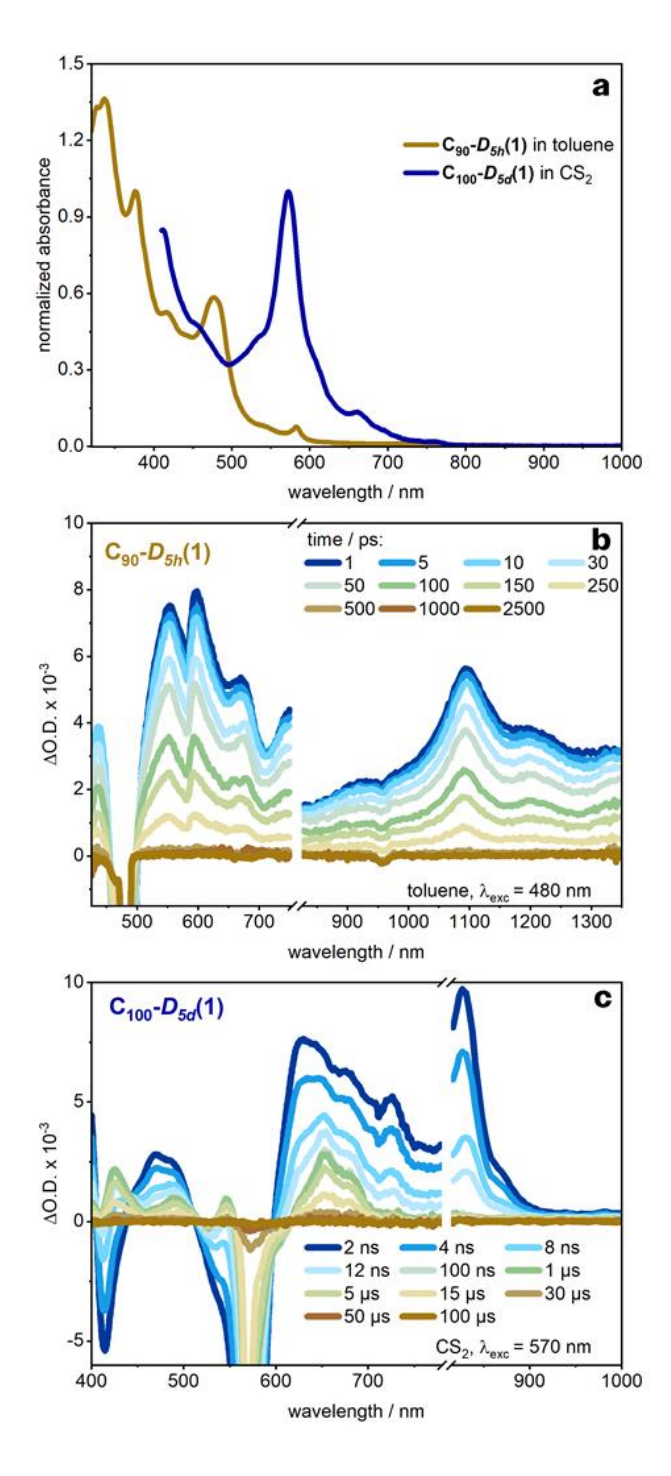


Figure 1. (a) Absorption spectra of D_{5h} - C_{90} in toluene (gold) and D_{5d} - C_{100} in CS₂ (blue) normalized to the 336 nm, and 573 nm maxima, respectively. (b) Differential absorption spectra on the subpicosecond (fs) time scale obtained from ultrafast transient absorption (TA) experiments (λ_{exc} = 480 nm) of D_{5h} - C_{90} in degassed toluene with several time delays between 1 and 2500 ps at room temperature. (c) Differential absorption spectra on the nanosecond time scale obtained from TA experiments (λ_{exc} = 570 nm) of D_{5d} - C_{100} in degassed CS₂ with several time delays between 2 ns and 100 μ s at room temperature. Time delays for (b) and (c) are given in the corresponding legends.

To put our experimental results into context, we further explored the trend of the HOMO–LUMO, optical, and electrochemical gaps within the series of tubular fullerenes between C_{60} and C_{150} with D_3 , $D_{3d/h}$, and $D_{5d/h}$ symmetry (see SI section 3.5). The gaps of tubular fullerenes with D_3 and $D_{3d/h}$ symmetry decrease continuously with increasing cage size. It is noteworthy that fullertubes of D_3 symmetry consistently have a lower gap than the $D_{3d/h}$ analogous with the same number of carbon atoms. Contrary to these findings, the gaps of the $D_{5d/h}$ series oscillate with a pattern repeating after every third species; for example, large gaps are found for D_{5h} - C_{70} and D_{5h} - C_{130} and small gaps for D_{5d} - C_{80} , D_{5h} - C_{110} , and D_{5d} - C_{140} (see Figures S22–S24).

In addition to the optical properties of the fullertubes, we were interested in their reduced and oxidized states. Differential pulse voltammetry (DPV) and cyclic voltammetry (CV) experiments in 1,2-dichlorobenzene (o-DCB) disclose two reversible reductions for D_{5h}-C₉₀ at -1.1 and -1.4 V versus Fc/Fc⁺ and a single oxidation at +0.6 V versus Fc/Fc⁺ yielding an electrochemical band gap of 1.7 eV (Figures S4 and S5). For D_{5d}-C₁₀₀, we find three reversible reductions at -1.1, -1.3, and -1.7 V versus Fc/Fc⁺ and one single oxidation at +0.9 V versus Fc/Fc⁺ resulting in an electrochemical band gap of 2.0 eV (Figures S6 and S7).

To calculate the first reductions and oxidations, we optimized the structures on the B3LYP/def2-SVP level of theory and described the solvent environment with the polarizable continuum model (PCM) o-DCB. ²¹ A thermodynamic correction of the zero-point energy was achieved by calculating the normal modes within the harmonic approximation. For D_{5h}-C₉₀, the calculated values are -0.97 and +0.73 eV versus Fc/Fc⁺ for the first reduction and oxidation, respectively. For D_{5d}-C₁₀₀, those are found at -1.04 and +0.85 eV versus Fc/Fc⁺. The calculated values are in near-perfect agreement with the experimental results, whereas deviations may probably stem from deficiencies within the PCM model or the neglecting of ion pairing effects.

To corroborate the conclusions drawn from the fluorescence measurements, we turned to ultrafast transient absorption (TA) pump–probe spectroscopy on the sub-pico- (fs-TAS) and -microsecond (μ s-TAS) time scales. For nonfluorescent D_{5h}-C₉₀, the differential TA spectra, which were recorded in toluene right after the 480 nm photoexcitation, include maxima at 434, 553, 595, 670, 760, 1098, and 1201 nm (see Figure 1b). Features in the near-infrared are broad in nature with a 1098 nm maximum. Notably, the maximum around 570 nm masks the bleaching due to ground-state absorption. From single-wavelength and global analyses we estimate that all of the aforementioned features decay with a lifetime of 125 ps. (Commencing with time delays of 800 ps, no transient absorption changes are discernible.) By virtue of a single species present that decays monoexponentially, we hypothesize that its origin is that of a singlet excited state. In line with the fluorescence assays, the decay is nonradiative without any significant intersystem crossing.¹⁵

Next, we carried out triplet–triplet energy transfer (TTET) experiments in toluene with anthracene as the energy donor and D_{5h} - C_{90} as the energy acceptor to generate triplet excited-state TA signatures. Figure S3 surveys μ s-TAS results for anthracene with a time delay of 3.00 μ s upon 387 nm photoexcitation in the absence and presence of D_{5h} - C_{90} . In the presence of D_{5h} - C_{90} , the differential TA spectrum gives rise to a 478 nm minimum, which is perfectly in line with the

corresponding steady-state absorption maximum of D_{5h} - C_{90} . Maxima are discernible at 574 and 890 nm, albeit broad and weak. From kinetic analyses, we confirm TTET; that is, the anthracene triplet excited state decay goes hand-in-hand with D_{5h} - C_{90} triplet excited state formation. The sensitized triplet excited state lifetime is 20.1 μ s, as determined by single wavelength analysis of the 890 nm time absorption profiles.

Turning to fs-TAS experiments with D_{5d} - C_{100} in CS_2 , immediately after 570 nm, photoexcitation maxima at 364, 684, and 828 nm are noted together with a minimum at 410 nm (see Figure 1c). Single-wavelength and global analyses resulted in a 5.54 ns lifetime of the underlying singlet excited state, a value that is in the typical range of singlet excited-state deactivation. A closer analysis of the fs-TAS reveals that the singlet excited-state decay coincides with the parallel formation of transient maxima at 420, 484, and 649 nm. From μ s-TAS, a dioxygen-sensitive lifetime of 15.4 μ s was determined (see Figure S11). This finding supports the notion that the decay is that of a triplet excited state. In TTET experiments with energy-donating anthracene, we found the same spectral characteristics. In σ -xylene, the same triplet excited-state fingerprints gave rise to a longer lifetime of 97.7 μ s (see Figure S12). (We attribute the shorter lifetime in CS_2 to residual dioxygen in the solvent and to lower viscosity compared to σ -xylene.)

In general, fullerenes are excellent electron acceptors. They are widely used as building blocks in energy-conversion schemes. SWCNTs, on the other hand, are better characterized as electron donors.^{22,23} D_{5d}-C₁₀₀ is the archetype fullertube, whose structure resembles that of a finite, endcapped (5,5)-armchair SWCNT. As such, we probed the electron-accepting properties of fullerenes and those of the electron-donating SWCNTs with, however, the same building block, that is, D_{5d}-C₁₀₀. To this end, we employed electron donating triethylamine (Et₃N) and electron accepting methylviologen (MV²⁺), respectively, in μs-TAS experiments (see Figure S13). (The lack of triplet excited states for D_{5h}-C₉₀ hampered any diffusion controlled electron transfer experiments.) Despite the presence of variable Et₃N concentrations, upon 570 nm photoexcitation in fs-TAS, the D_{5d}-C₁₀₀ singlet excited state is seen to transform to the corresponding triplet excited state. It is important that the intersystem crossing dynamics remain virtually unchanged even in the presence of 10⁻⁴ M Et₃N. However, the triplet excited-state fingerprints are subject to a faster decay. For example, rather than seeing a 15.4 µs lifetime in the absence of any Et₃N, vide supra, it takes 1.70 μ s in the presence of 10^{-4} M Et₃N, by which the 425, 490, 547, 648, and 681 nm maxima are replaced by 432, 498, and 617 nm maxima. The latter are assigned to the one-electron reduced form of D_{5d}-C₁₀₀. Given that the oxidation of the strongly electron donating Et₃N occurs at +0.69 V versus SCE, ^{24,25} together with the D_{5d}-C₁₀₀ reduction of -0.7 V vs SCE, we postulate a thermodynamically driven hole transfer from the triplet excited state of D_{5d}-C₁₀₀ to Et₃N. In contrast, no detectable changes were noted at MV²⁺ concentrations as high as 10⁻⁴ M. Here, the reduction of the electron accepting MV²⁺ at -0.69 V vs SCE^{26} together with the oxidation of D_{5d} - C_{100} at +1.3 V vs SCE are, however, unfavorable to electron transfer. (Values were converted to V versus SCE using the conversion E°_{1/2} (Fc/Fc⁺) = +0.40 vs SCE.)

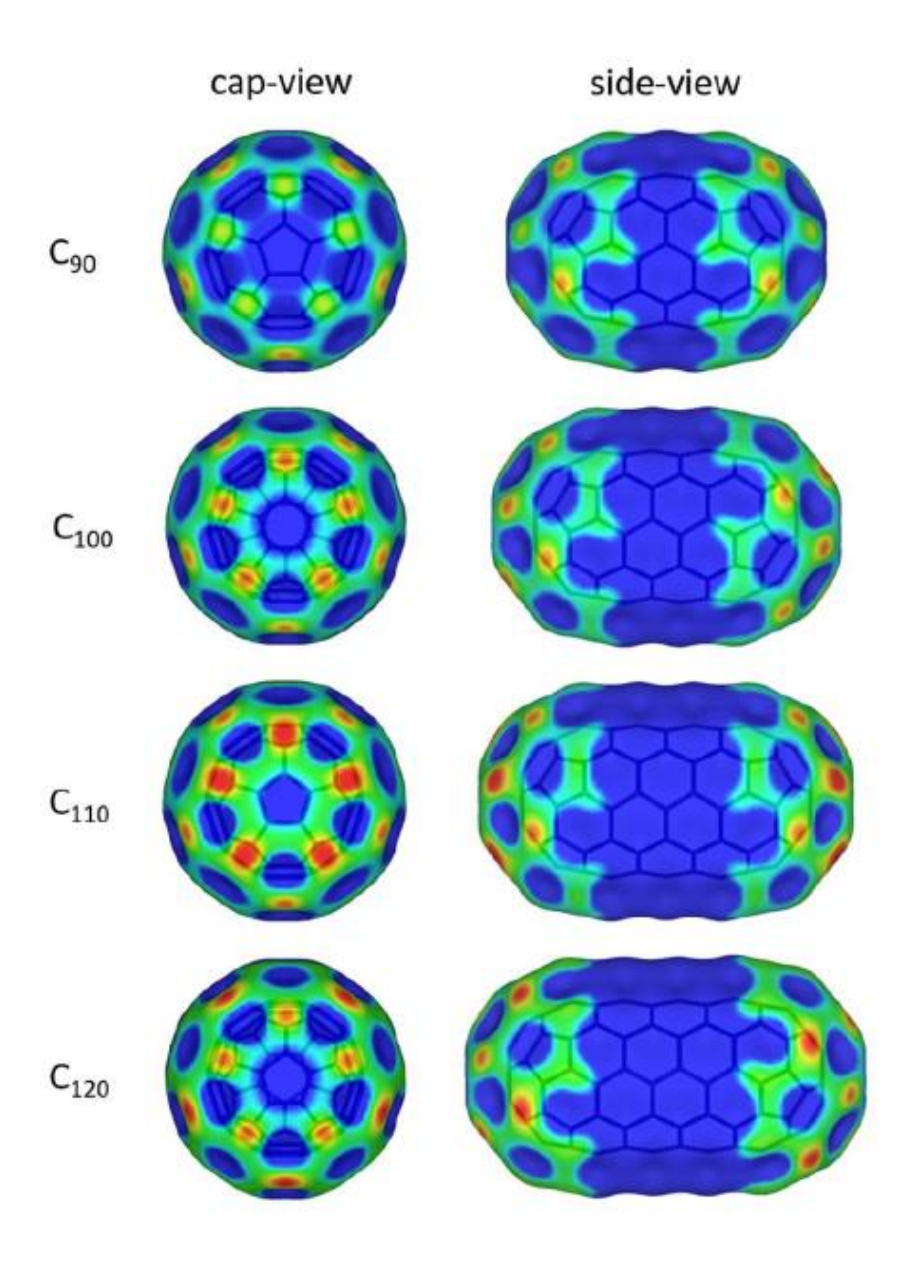


Figure 2. Electrostatic potential (red: -0.0025; blue: +0.0025 au) of D_{5h} - C_{90} , D_{5d} - C_{100} , D_{5h} - C_{110} , and D_{5d} - C_{120} mapped on the electron density isosurface (0.001 au). Calculations performed with BLYP/def2-SVP in the gas phase.

Recently, the importance of charge distribution within D_{5h} - C_{90} was highlighted to govern the cocrystallization with electron-rich nickel-porphyrins (NiP). NiP interacts preferentially with the side of D_{5h} - C_{90} , where the electrostatic potential is positive. This contrasts to the caps with their negative electrostatic potentials. We repeated these calculations for D_{5h} - C_{90} , D_{5d} - C_{100} , D_{5h} - C_{110} , and D_{5d} - C_{120} at the BLYP/def2SVP level, and the resulting electrostatic potential maps are shown in Figure 2. The corresponding plots suggest that D_{5h} - C_{90} , D_{5d} - C_{110} , and D_{5d} - C_{120} are best described as two C_{60} caps with negative potentials connected by the same cycloparaphenylenes with positive potentials. Such large areas of positive potential are promising for a complexation

with, for example, cycloparaphenylenes (CPPs). CPPs not only are shape complementary but also feature negative electrostatic potentials on their concave sides.²⁷ We therefore hypothesize a significant stability of CPP complexation with longer fullertubes. These experiments are the focal point of ongoing studies.

Supporting Information

The Supporting Information is available free of charge at https://pubs.acs.org/doi/10.1021/jacs.2c02442.

Instrumentation, experimental procedures, photophysical and electrochemical measurements, and additional spectra, computational details and further information: functional screening, xyz coordinates, calculated gaps, optimized structures.

Author Contributions

C.M.S. and M.K. contributed equally.

Notes

The authors declare no competing financial interest.

Acknowledgments

S.S. thanks the National Science Foundation Grant 1856461 for financial support.

References

- (1) Ajie, H.; Alvarez, M. M.; Anz, S. J.; Beck, R. D.; Diederich, F.; Fostiropoulos, K.; Huffman, D. R.; Krätschmer, W.; Rubin, Y.; Schriver, K. E.; Sensharma, D.; Whetten, R. L. Characterization of the Soluble All-Carbon Molecules C₆₀ and C₇₀. *J. Phys. Chem.* **1990**, 94 (24), 8630–8633.
- (2) Krätschmer, W.; Fostiropoulos, K.; Huffman, D. R. The Infrared and Ultraviolet Absorption Spectra of Laboratory-Produced Carbon Dust: Evidence for the Presence of the C₆₀ Molecule. *Chem. Phys. Lett.* **1990**, 170 (2–3), 167–170.
- (3) Krätschmer, W.; Lamb, L. D.; Fostiropoulos, K.; Huffman, D. R. Solid C₆₀: A New Form of Carbon. *Nature* **1990**, 347 (6291), 354–358.
- (4) Hirsch, A. The Era of Carbon Allotropes. *Nat. Mater.* **2010**, 9 (11), 868–871.
- (5) Lu, X.; Akasaka, T.; Nagase, S. Soluble and Tubular Higher Fullerenes That Encapsulate Metals. *Angew. Chemie Int. Ed.* **2012**, 51 (12), 2812–2814.
- (6) Beavers, C. M.; Jin, H.; Yang, H.; Wang, Z.; Wang, X.; Ge, H.; Liu, Z.; Mercado, B. Q.; Olmstead, M. M.; Balch, A. L. Very Large, Soluble Endohedral Fullerenes in the Series La₂C₉₀ to La₂C₁₃₈: Isolation and Crystallographic Characterization of La₂@D₅(450)-C₁₀₀. J. Am. Chem. Soc. 2011, 133 (39), 15338–15341.
- (7) Fritz, M. A.; Kemnitz, E.; Troyanov, S. I. Capturing an Unstable C_{100} Fullerene as Chloride, $C_{100}(1)Cl_{12}$, with a Nanotubular Carbon Cage. *Chem. Commun.* **2014**, 50 (93), 14577–14580.

- (8) Yang, S.; Wang, S.; Troyanov, S. I. The Most Stable Isomers of Giant Fullerenes C_{102} and C_{104} Captured as Chlorides, $C_{102}(603)$ - $Cl_{18/20}$ and $C_{104}(234)Cl_{16/18/20/22}$. Chem. A Eur. J. **2014**, 20 (23), 6875–6878.
- (9) Wang, S.; Yang, S.; Kemnitz, E.; Troyanov, S. I. New Giant Fullerenes Identified as Chloro Derivatives: Isolated-Pentagon-Rule C₁₀₈(1771)Cl₁₂ and C₁₀₆(1155)Cl₂₄ as Well as Nonclassical C₁₀₄Cl₂₄. *Inorg. Chem.* **2016**, 55 (12), 5741–5743.
- (10) Cai, W.; Li, F. F.; Bao, L.; Xie, Y.; Lu, X. Isolation and Crystallographic Characterization of $La_2C_2@C_s(574)-C_{102}$ and $La_2C_2@C_2(816)-C_{104}$: Evidence for the Top-Down Formation Mechanism of Fullerenes. *J. Am. Chem. Soc.* **2016**, 138 (20), 6670–6675.
- (11) Rodríguez-Fortea, A.; Balch, A. L.; Poblet, J. M. Endohedral Metallofullerenes: A Unique Host–Guest Association. *Chem. Soc. Rev.* **2011**, 40 (7), 3551–3563.
- (12) Koenig, R. M.; Tian, H. R.; Seeler, T. L.; Tepper, K. R.; Franklin, H. M.; Chen, Z. C.; Xie, S. Y.; Stevenson, S. Fullertubes: Cylindrical Carbon with Half-Fullerene End-Caps and Tubular Graphene Belts, Their Chemical Enrichment, Crystallography of Pristine C₉₀-D_{5h}(1) and C₁₀₀-D_{5d}(1) Fullertubes, and Isolation of C1₀₈, C₁₂₀, C₁₃₂, and C₁₅₆ Cages of Unknown Structure. *J. Am. Chem. Soc.* **2020**, 142 (36), 15614–15623.
- (13) Stevenson, S.; Liu, X.; Sublett, D. M.; Koenig, R. M.; Seeler, T. L.; Tepper, K. R.; Franklin, H. M.; Wang, X.; Huang, R.; Feng, X.; Cover, K.; Troya, D.; Shanaiah, N.; Bodnar, R. J.; Dorn, H. C. Semiconducting and Metallic [5,5] Fullertube Nanowires: Characterization of Pristine D_{5h}(1)-C₉₀ and D_{5d}(1)-C₁₀₀. J. Am. Chem. Soc. 2021, 143 (12), 4593–4599.
- (14) Yang, H.; Beavers, C. M.; Wang, Z.; Jiang, A.; Liu, Z.; Jin, H.; Mercado, B. Q.; Olmstead, M. M.; Balch, A. L. Isolation of a Small Carbon Nanotube: The Surprising Appearance of D_{5h}(1)-C₉₀. *Angew. Chemie Int. Ed.* **2010**, 49 (5), 886–890.
- (15) Liu, Y.; Lin, M.; Zhao, Y. Intersystem Crossing Rates of Isolated Fullerenes: Theoretical Calculations. *J. Phys. Chem. A* **2017**, 121 (5), 1145–1152.
- (16) Yumura, T.; Hirahara, K.; Bandow, S.; Yoshizawa, K.; Iijima, S. A Theoretical Study on the Geometrical Features of Finite-Length Carbon Nanotubes Capped with Fullerene Hemisphere. *Chem. Phys. Lett.* **2004**, 386 (1–3), 38–43.
- (17) Lee, C.; Yang, W.; Parr, R. G. Development of the Colle-Salvetti Correlation-Energy Formula into a Functional of the Electron Density. *Phys. Rev. B* **1988**, 37 (2), 785–789.
- (18) Becke, A. D. Density-Functional Thermochemistry. III. The Role of Exact Exchange. *J. Chem. Phys.* **1993**, 98 (7), 5648–5652.
- (19) Staroverov, V. N.; Scuseria, G. E.; Tao, J.; Perdew, J. P. Comparative Assessment of a New Nonempirical Density Functional: Molecules and Hydrogen-Bonded Complexes. *J. Chem. Phys.* **2003**, 119 (23), 12129–12137.
- (20)Adamo, C.; Barone, V. Toward Reliable Density Functional Methods without Adjustable Parameters: The PBE0Model. *J. Chem. Phys.* **1999**, 110 (13), 6158–6170.
- (21) Tomasi, J.; Mennucci, B.; Cammi, R. Quantum Mechanical Continuum Solvation Models. *Chem. Rev.* **2005**, 105, 2999–3093.
- (22) Guldi, D. M.; Rahman, G. M. A.; Zerbetto, F.; Prato, M. Carbon Nanotubes in Electron Donor Acceptor Nanocomposites. *Acc. Chem. Res.* **2005**, 38 (11), 871–878.
- (23) D'Souza, F.; Ito, O. Supramolecular Donor-Acceptor Hybrids of Porphyrins/Phthalocyanines with Fullerenes/Carbon Nanotubes: Electron Transfer, Sensing, Switching, and Catalytic Applications. *Chemical Communications.* **2009**, 4913–4928.

- (24) Chow, Y. L.; Danen, W. C.; Nelsen, S. F.; Rosenblatt, D. H. Nonaromatic Aminium Radicals. *Chem. Rev.* **1978**, 78 (3), 243–274.
- (25) Pellegrin, Y.; Odobel, F. Les Donneurs d'électron Sacrificiels Pour La Production de Combustible Solaire. C. R. Chim. **2017**, 20 (3), 283–295.
- (26) Heyrovský M. The Electroreduction of Methyl Viologen. *J. Chem. Soc. Chem. Commun.* **1987**, 24, 1856–1857.
- (27) Fomine, S.; Zolotukhin, M. G.; Guadarrama, P. Russian Doll Complexes of [n]Cycloparaphenylenes: A Theoretical Study. *J. Mol. Model.* **2012**, 18 (9), 4025–4032.